鳥取大学研究成果リポジトリ
Tottori University research result repository

タイトル Title	Keggin-type molybdovanadophosphoric acids loaded on ZSM-5 zeolite as a bifunctional catalyst for oxidehydration of glycerol
著者 Auther(s)	Suganuma, Satoshi; Hisazumi, Takuya; Taruya, Kohtaro; Tsuji, Etsushi; Katada, Naonobu
掲載誌・巻号・ページ Citation	Molecular Catalysis , 449 : 85 - 92
刊行日 Issue Date	2018-04-30
資源タイプ Resource Type	学術雑誌論文 / Journal Article
版区分 Resource Version	著者版 / Author
権利 Rights	© 2018 Elsevier B.V. All rights reserved.
DOI	10.1016/j.mcat.2018.02.015
URL	https://repository.lib.tottori-u.ac.jp/7093

Keggin-type molybdovanadophosphoric acids loaded on ZSM-5 zeolite as a bifunctional catalyst for oxidehydration of glycerol

Satoshi Suganuma*[1], Takuya Hisazumi[2], Kohtaro Taruya[2], Etsushi Tsuji[2] and Naonobu Katada[2]

1 Center for Research on Green Sustainable Chemistry, Graduate School of Engineering, Tottori University, 4-101 Koyama-cho Minami, Tottori 680-8552, Japan

2 Department of Chemistry and Biotechnology, Graduate School of Engineering, Tottori University, 4-101 Koyama-cho Minami, Tottori 680-8552, Japan

* E-mail: suganuma@chem.tottori-u.ac.jp, Tel.: +81 (857) 31-5256, Fax: +81 (857) 31-5684

Abstract

Glycerol is a promising renewable feedstock for the manufacture of C3 derivatives. We investigated the one-pass oxidehydrarion of glycerol through the dehydration of glycerol into acrolein, followed by the oxidation of acrolein. A novel bifunctional catalyst for this reaction was prepared by loading the Keggin-type molybdovanadophosphoric acid $H_{3+x}PV_xMo_{12-x}O_{40}$ (x = 0-3) on ZSM-5 (MFI) zeolite (Si/Al = 45) exhibiting both dehydration and oxidation activity. $H_5PV_2Mo_{10}O_{40}$ and $H_6PV_3Mo_9O_{40}$ were stable and dispersed on ZSM-5 zeolite, and the acidic property of the ZSM-5 zeolite was retained. The oxidehydration of glycerol was catalyzed by $H_5PV_2Mo_{10}O_{40}$ loaded on the ZSM-5 zeolite with high selectivity of acrylic acid. *In-situ* IR analysis suggests that acrolein molecules adsorbed on $H_5PV_2Mo_{10}O_{40}$/ZSM-5 were converted into acrylic acid due to the inhibition of side-reactions such as polymerization and auto-condensation, which induced coke formation, compared with the other Mo and V-based oxides loaded on ZSM-5 zeolite.

1. Introduction

Petroleum is a limited resource that has been a vital feedstock for the manufacture of liquid fuels and petrochemicals, but there is increasing interest in the world centering on countries with agriculture-based economics to use biomass as a renewable resource. Biodiesel as an alternative fuel comprises fatty acid esters and is typically produced through the transesterification of vegetable fats or oils with alcohol [1]. The production of biodiesel is increasing, and simultaneously the process induced the fact that ca. 10 wt% of glycerol is being generated as a byproduct during transesterification [2]. Residual glycerol has been burned for thermal power generation, but it is demanded to use it as a feedstock for the manufacture of several C3 derivatives [3]. There are approximately 1,500 products currently marketed that contain glycerol, such as cosmetics, pharmaceuticals, and food products [4]. Glycerol contains three hydroxyl groups, which offer diverse opportunities for catalytic conversion into high-value chemicals. The conversion of glycerol into value-added products would improve the economics of biodiesel production and thus approaches for the transformation of glycerol would be a key development towards alternative bio-based energy resources and chemicals.

Glycerol dehydration followed by oxidation generates acrylic acid, which is a widely used intermediate in the manufacture of water-absorbing polymers, paints, plastics, and

rubber [5 - 7]. Acrylic acid is typically produced through the two-step oxidation of propylene, a petroleum feedstock. Propylene is oxidized to acrolein, then further oxidized into acrylic acid. Over 3 million tons per year of acrylic acid are manufactured using this approach and is increasing annually. Using glycerol as a bio-based feedstock in the manufacture of acrylic acid is therefore desirable to meet this growing demand.

Glycerol is typically converted into acrylic acid through multiple steps of dehydration and subsequent selective oxidation, but acrolein generated in the first reaction is difficult to store in chemical plants due to its high reactivity, toxicity, and combustibility. The direct oxidehydration of glycerol generates acrylic acid, eliminating the need to store acrolein. However, realization of this challenging reaction requires a bifunctional catalyst with acid sites (probably Brønsted type) for the dehydration of glycerol and selective oxidation properties for the conversion of acrolein into acrylic acid. The oxidehydration of glycerol can be catalyzed by bifunctional catalysts [8 - 13] which contain vanadium as a redox center to stabilize acrolein in the form of acrylate [14]. Furthermore, the addition of molybdenum and/or tungsten likely induces the generation of acidic sites. In particular, the catalytic activity of W-V mixed oxides with a hexagonal tungsten bronze structure can be improved by the addition of niobium, which generates acidic properties [11]. Vanadium oxide loaded on ZSM-5 zeolite, with negligible

deactivation during the dehydration of glycerol [15], has been investigated for the oxidehydration of glycerol [16]. However, this approach provided only moderate yields of acrylic acid. Conversely, vanadium-substituted cesium salts (Keggin-type heteropoly acids) have been reported to exhibit high selectivity towards acrylic acid in the oxidehydration of glycerol, although catalytic activity gradually decreases [17].

In this work, we synthesized a novel catalyst for oxidehydration by loading the Keggin-type molybdovanadophosphoric acid $H_{3+x}PV_xMo_{12-x}O_{40}$ (x = 0-3) onto ZSM-5 zeolite. This catalyst shows high dispersion and stability of the heteropoly acid. A single-bed reactor loaded with this catalyst exhibits higher reaction rate to the desired product than mixture and dual-bed reactors comprising ZSM-5 zeolite and $H_5PV_2Mo_{10}O_{40}/SiO_2$. To our knowledge, this study is the first example using a heteropoly acid combined with ZSM-5 zeolite for the direct oxidehydration of glycerol. In addition, *in-situ* IR analysis of the adsorption of acrolein or acrylic acid on the catalyst and the oxidation of acrolein by the catalyst will give new insights into the catalytic properties required for the oxidehydration of glycerol.

2. Experimental

2.1 Catalyst preparation

$H_{3+x}PV_xMo_{12-x}O_{40}$ (x = 0-3, Japan New Metal), vanadium (IV) oxide sulfate n-hydrate (99.9%, Wako) and hexaammonium heptamolybdate tetrahydrate (99.0%, Wako) were used without further purification. ZSM-5 and SiO_2 were provided by the Catalysis Society of Japan (JRC-Z5-90NA(1) (Na-form, Si/Al = 45) and JRC-SIO-13, respectively). The Na-form zeolite was ion-exchanged into the NH_4-form by stirring in a 5 wt% ammonium nitrate solution (NH_4/Na = 10 in the system) at 353 K for 4 h, filtered then washed with water 3 times. These procedures (stirring, filtering and washing) were repeated 3 times. The zeolite was dried at 383 K overnight to provide NH_4-form zeolite. H-form zeolite was prepared by calcination of it at 823 K in air.

In a typical procedure, 90 μmol of $H_{3+x}[PV_xMo_{12-x}O_{40}] \cdot nH_2O$ (x = 0-3) was dissolved in 100 mL of distilled water with stirring. After adding 1.0 g of ZSM-5 zeolite, the suspension was evaporated to dryness, and the powder was dried at 383 K in air for 12 h. The catalysts were calcined at 573 K for 3 h in air. The product contained 17-18 wt% $H_{3+x}[PV_xMo_{12-x}O_{40}]$ and was designated "PV_xMo_{12-x}/ZSM-5". PV_2Mo_{10}/SiO_2 was prepared from SiO_2 and $H_5[PV_2Mo_{10}O_{40}] \cdot nH_2O$ using the same procedure. Mo-V/ZSM-5 without Keggin structure for comparison was prepared through the impregnation of Mo-

V mixed oxides. Hexaammonium heptamolybdate tetrahydrate (120 μmol) and 240 μmol of vanadium (IV) oxide sulfate n-hydrate were dissolved in 100 mL of distilled water with stirring. After adding 1.0 g of ZSM-5 zeolite, the suspension was evaporated to dryness and the powder was dried at 383 K in air for 12 h. The catalysts were calcined at 573 K for 3 h in air. Mo-V/ZSM-5 contained the same amount of ([Mo]+[V]) as PV_xMo_{12-x}/ZSM-5 and PV_2Mo_{10}/SiO_2.

2.2 Characterization of the catalysts

The crystalline phases of the catalysts were analyzed by X-ray diffraction using a Rigaku Ultima IV diffractometer, with Cu Kα radiation. Data were collected in the 2θ range from 5 to 50 degrees. The N_2 adsorption-desorption isotherms were determined on a BELSORP-max apparatus (MicrotracBEL). The samples were pretreated at 573 K under vacuum for 1 h before measurement. Raman spectra were recorded using a JASCO NRS-7100 at a wavenumber of 785 nm with a CCD detector in air. Thermogravimetry/differential thermal analyses (TG-DTA) were determined on a Rigaku Thermos Plus instrument. Samples were heated from 313 to 1073 K at a rate of 10 K min^{-1}. SEM (scanning electron microscope) images were collected using a Hitachi S-4800 SEM with EDX (Energy Dispersive X-ray) spectrometry.

Ammonia infrared-mass spectroscopy/temperature programmed desorption (IRMS-TPD) analysis for the measurement of acidic properties [18] was conducted on an automatic IRMS-TPD analyzer (MicrotracBEL). Powders of the catalysts were compressed at 20 MPa into self-supporting disks 1 cm in diameter and pre-treated in a stream of oxygen (37 μmol s^{-1}, 100 kPa) at 623 K for 1 h in an IR cell. The sample was heated at a ramp rate of 2 K min^{-1} from 343 to 623 K under a helium stream (89 μmol s^{-1}, 6.0 kPa) and IR spectra were collected at 1 K intervals. Next, ammonia was adsorbed at 343 K, and heating and IR spectrum collection under a helium stream were conducted as the temperature was raised from 343 to 803 K. The concentration of ammonia in the gas phase was monitored by a mass spectrometer (MS) operating at $m/e = 16$. The amount of acidic sites was calculated from the intensity of desorbed ammonia in the TPD spectrum.

2.3 Gas-phase conversion of glycerol into acrylic acid

The activity of each catalyst for the oxidehydration of glycerol was assessed by packing 0.45 g of the catalyst with 0.10 g of glass beads into a Pyrex tube (i.d. 10 mm). The temperature of the catalyst bed was monitored by a thermocouple located inside the catalyst bed, and the temperature of this thermocouple was controlled at 623 K. The gas

flow was kept at 1.8 L h^{-1} and its composition was O_2 (21 mol%) and N_2 (79 mol%).

Glycerol aqueous solution (30 wt%) were fed at 1.5 g h^{-1}; glycerol and water were

vaporized in the gas flow before the catalyst bed. The molar ratio of glycerol/H_2O/O_2/N_2

was 4.9/58/16/58. The outlet effluent was trapped by water at 273 K after the system had

stabilized for 0.5 h at 623 K. The products were analyzed by a gas chromatograph (GC)

(Shimadzu GC-2014) with a capillary column (TC-WAX) using a flame ionization

detector (FID) and a packed column (WG-100) using a thermal conductivity detector

(TCD). The untrapped gas products were analyzed through a six-way valve in the online

FID-GC system, and the collected CO_x (CO and CO_2) with gas-tight syringe was analyzed

by the TCD-GC system.

2.4 *In-situ* IR analysis of acrolein adsorbed on the catalysts

    In-situ IR analysis of molecules adsorbed on the catalyst samples was carried out

using an automatic IRMS-TPD analyzer (MicrotracBEL). Catalyst powders were

compressed at 20 MPa into self-supporting disks 1 cm in diameter and pre-treated at 373

K under vacuum for 1 h in an IR cell to remove adsorbed water. Acrolein or acrylic acid

was adsorbed at 303 K, and IR spectra were collected as 21 mol% of O_2/N_2 (0.24 L h^{-1})

at 70 Pa was streamed over the sample and the temperature was increased at a ramp rate

of 2 K min^{-1} from 303 to 673 K.

3. Results and discussion

3.1 Characterization

Fig. 1 shows the XRD patterns of ZSM-5 zeolites before and after loading PV_xMo_{12-x} or Mo-V mixed oxide, and of SiO_2 before and after loading PV_2Mo_{10}. The diffraction peaks of the ZSM-5 zeolite support indicated an MFI zeolitic framework structure (**Fig. 1** (a)). Loading PV_xMo_{12-x} on the support did not change the zeolitic structure (**Fig. 1** (b)-(d)). The introduction of PV_xMo_{12-x}, $x = 0–2$, resulted in a small peak at about 6 degrees and likely indicates a periodic three-dimensional structure in small aggregates of the heteropoly acids. This signal was not observed in the PV_3Mo_9/ZSM-5 pattern (**Fig. 1** (e)). The zeolitic structures in Mo-V/ZSM-5 was not collapsed, and periodic crystal structures of the Mo and/or V oxides were not observed (**Fig. 1** (f)). The SiO_2 pattern before and after loading PV_2Mo_{10} showed an amorphous structure (**Fig. 1** (g)-(h)). However, Keggin structure and the other crystalline structure of Mo and V-based oxides were not appeared in XRD patterns, indicating the lack of large crystallites of these materials. **Fig. 2** shows representative nitrogen adsorption-desorption isotherms. The steep increases at very low relative pressure ($p/p_0 < 0.1$) and high relative pressure ($p/p_0 > 0.4$) in the bare ZSM-5 zeolite were associated with microporosity and mesoporosity (**Fig. 2** (a)). These features did not change after loading PV_xMo_{12-x} or Mo-V mixed oxide (**Fig. 2** (b)-(f)). The

11

heteropoly acids and the Mo-V mixed oxide were thus dispersed on the ZSM-5 zeolite

and SiO_2. **Fig. 3** shows SEM images and the corresponding EDX mapping images of

PV_2Mo_{10}/ZSM-5 and ZSM-5 alone; each have a particle size of about 20 μm. The EDX

mapping images of PV_2Mo_{10}/ZSM-5 show silicon, molybdenum, aluminum, and a small

amount of vanadium, suggesting that PV_2Mo_{10} is probably uniformly supported on the

outer surface of ZSM-5 zeolite particles because the primary structure of the

heteropolyacid (ca. 1 nm) cannot enter the micropores of the MFI zeolite structures.

Raman spectra of the catalysts are presented in **Fig. 4**. The Raman spectra of ZSM-

5 zeolite and supported zeolites show a band around 364 cm^{-1}, assigned to v_s (Si-O-Si)

modes due to framework vibration of five-membered rings in the MFI crystals [19,20].

The band at 1003 cm^{-1}, with a shoulder band at 986 cm^{-1}, and the bands at 608 and 250

cm^{-1}, were assigned to the terminal Mo=O stretching vibration mode, Mo-O-Mo

stretching vibration mode, and Mo-O-Mo bending vibration mode of the intact Keggin-

type heteropoly acid, respectively [21-23]. Additional bands at 980, 815, 670 and 290

cm^{-1} were observed in the Raman spectra of PMo_{12} and $PVMo_{11}$ loaded on ZSM-5 zeolite

and arose from asymmetric O=Mo=O, symmetric O=Mo=O and symmetric Mo-O-Mo

stretching modes, and the O=Mo=O wagging mode of MoO_3, respectively [24,25] (**Fig.**

4 (b)-(c)). Therefore, some heteropoly acids on these catalysts had decomposed into

12

molybdenum oxides. However, no band assignable to vibration modes of V_2O_5 was observed. In contrast, PV_2Mo_{10} and PV_3Mo_9 were stable, and the structure of the Keggin-type heteropoly acids was retained on ZSM-5 zeolite and SiO_2 (**Fig. 4** (d)-(f)). In the Raman spectrum of Mo-V/ZSM-5 (**Fig. 4** (g)), the bands at 980, 670, 290 and 240 cm^{-1} were ascribed to MoO_3, and the bands at 894, 885 and 836 cm^{-1} were likely due to a MoO_x ($x < 3$)-type structure [24, 25]. Fig. S1 shows TG-DTA curves. Mass loss below 523 K was presumably due to removal of adsorbed water.

The acidic properties of the catalysts influence catalytic performance during glycerol dehydration, as reported [15].　The ammonia IRMS-TPD was used to quantify the Brønsted or Lewis acid sites [26]. IR spectra of the 1050-1700 cm^{-1} region of NH_3 adsorbed on the catalysts are shown in Fig. S2. After pretreatment under a stream of helium at 623 K and cooling to 343 K, the reference spectrum was measured under a stream of helium while increasing the temperature. This reference spectrum was subtracted from the sample spectrum after adsorption of NH_3, recorded in the same atmosphere at the same temperature. The bands corresponding to the adsorbed NH_3 bending modes were assigned as reported [26]. The bands around 1450 and 1625 cm^{-1} were assigned according to the literature [18] to the ν_4 bending mode of symmetric NH_4 adsorbed on Brønsted acid sites and the δ_s of asymmetric NH_3 bending modes

13

coordinatively adsorbed on Lewis acid sites, respectively. The band assignable to ammonia bound to Brønsted acid sites was observed for all the catalysts, while the band assignable to ammonia coordinatively adsorbed on Lewis acid sites was rarely observed. The amounts of Brønsted acid sites were determined by the IRMS-TPD profile [26] and are shown in **Table 1**, on the assumption in which MS-TPD showed the sum of TPD profiles of the observed Brønsted acid sites. The amount of Brønsted acid sites on PMo_{12} and $PVMo_{11}$ loaded on ZSM-5 was less than that on the parent ZSM-5 alone, while PV_2Mo_{10}, PV_3Mo_9 and Mo-V mixed oxide loaded on ZSM-5 provided the similar amount of Brønsted acid sites to the parent ZSM-5. PV_2Mo_{10}/SiO_2 had no or very weak Brønsted acid sites, therefore dehydration of glycerol cannot proceed over PV_2Mo_{10}.

3.2 Oxidehydration of glycerol

The oxidehydration of glycerol was performed under gas-phase conditions with PV_xMo_{12-x}/ZSM-5, containing a total amount of 0.90 mol kg^{-1} of [Mo] and [V]. The catalytic behaviors were studied as a function of time on stream (**Fig. 5**). Complete conversion of glycerol was obtained with all catalysts (**Fig. 5** (a)). The yield of acrolein for $PVMo_{11}/ZSM$-5 was lower than that for PMo_{12}/ZSM-5 (**Fig. 5** (b)). An increase in the vanadium content in the heteropoly acids on the catalysts resulted in a decrease in acrolein

14

yield. The yield of acrylic acid increased with introduction of V as the acrolein yield decreased (**Fig. 5** (c)). An increase in the vanadium content in the catalysts enhanced the catalytic activity for the sequential oxidation of acrolein, with an exception of PV_3Mo_9/ZSM-5. Acetol formed via dehydration of the primary hydroxyl group in glycerol likely continuously decomposed into acetaldehyde, which was also oxidized into acetic acid [27, 28]. As shown in **Fig. 5** (d) and (e), the yields of acetaldehyde and acetic acid were much lower than those of acrolein and acrylic acid. An increase in the vanadium content of the catalysts resulted in a decrease in the acrolein and acetaldehyde yields and promoted the formation of acrylic acid and acetic acid. Vanadium can induce the oxidation of C3 and C2 aldehydes into carboxylic acids. Fig. S3 shows TG-DTA curves of collected PV_xMo_{12-x}/ZSM-5 after the reaction. The weight loss in the range 300-700 K and 700-900 K indicated elimination of water and carbon deposit. There is not the difference of the amounts of water and carbon deposit between the catalysts, and the amounts was estimated at about 1 and 2 %, respectively. The carbon deposit at 6 h was slight amount, therefore there is not effect on catalytic activity. PV_2Mo_{10} and PV_3Mo_9 loaded on ZSM-5 zeolite were more stable than PMo_{12} and $PVMo_{11}$, as shown by the Raman spectra in the previous section, and thus PV_2Mo_{10} and PV_3Mo_9 on ZSM-5 zeolite likely contain larger amount of active sites for the oxidation reaction. The high yield of

15

acrylic acid was thus obtained in the oxidehydration of glycerol by a more balance of the

2 Brønsted acid sites and stable heteropoly acids on PV_2Mo_{10}/ZSM-5, and therefore the

3 catalytic performance of PV_2Mo_{10}/ZSM-5 was investigated in detail.

4   The effect of the loading amount of PV_2Mo_{10} on the conversion and yield of products

5 in the oxidehydration of glycerol at 6 h of the time on stream is shown in **Fig. 6**. Complete

6 conversion of glycerol was achieved on all the catalysts. PV_2Mo_{10} (5.8 wt%; 0.36 mol kg^{-1}

7 of ([Mo] + [V]) content) loaded on ZSM-5 zeolite provided a high yield of the aldehydes

8 such as acrolein (ca. 60%) and acetaldehyde (ca. 16%), but low yield of the carboxylic

9 acids such as acrylic acid and acetic acid. An increase in the amount of PV_2Mo_{10} resulted

10 in decrease of the yields of the aldehydes but increased the yields of the carboxylic acids.

11 The highest yield of acrylic acid (31%) was obtained by using 17.3 wt% of PV_2Mo_{10} (1.08

12 mol kg^{-1} of ([Mo] + [V]) content) loaded on ZSM-5 zeolite. However, the excess amount

13 of PV_2Mo_{10} resulted in a slightly decreased yield of acrylic acid and decreased the yield

14 of acrolein down to ca. 15%. PV_2Mo_{10} (17.3 wt%) loaded on ZSM-5 zeolite provided the

15 highest total yield of acrolein and acrylic acid.

16   The combination of oxidation catalyst (heteropoly acids) and acid catalyst (zeolite)

17 to form a bifunctional catalyst is the aim of this study. To clarify the effect of PV_2Mo_{10}

18 loading on catalytic performance for the oxidehydrarion of glycerol, we here compared

16

1   PV_2Mo_{10}/SiO_2, Mo-V/ZSM-5, a physically mixed catalyst (0.39 g of ZSM-5 zeolite +

2   0.45 g of PV_2Mo_{10}/SiO_2 (17.3 wt%)), a separate sequential bed (1st bed: 0.39 g of ZSM-

3   5 zeolite, 2nd bed: 0.45 g of PV_2Mo_{10}/SiO_2 (17.3 wt%)), and $PV_2Mo_{10}/ZSM-5$.

4   PV_2Mo_{10}/SiO_2 and Mo-V/ZSM-5 contained the same amount of [Mo] + [V] on

5    $PV_2Mo_{10}/ZSM-5$. **Fig. 7** shows time courses for the oxidehydration of glycerol by the

6   various catalytic systems, as described above. Full conversion was obtained with all the

7   systems (**Fig. 7** (a)). PV_2Mo_{10}/SiO_2 provided a much low yield of acrolein and acrylic

8   acid compared to the other catalysts. The negligible glycerol was dehydrated on

9   PV_2Mo_{10}/SiO_2 with very weak Brønsted acid sites, but the other products were formed

10   through oxidation. The physically mixed catalyst resulted in the formation of more

11   acrolein and acrylic acid than PV_2Mo_{10}/SiO_2. Glycerol was dehydrated into acrolein over

12   ZSM-5 zeolite, and acrolein was then oxidized into acrylic acid over PV_2Mo_{10}/SiO_2.

13   Locating ZSM-5 zeolite and PV_2Mo_{10}/SiO_2 into the separate bed increased the yield of

14   acrolein and acrylic acid compared to the mixed bed. $PV_2Mo_{10}/ZSM-5$ was observed to

15   be most active for the production of acrylic acid, resulting in the high yield of acrolein

16   and acrylic acid. Mo-V/ZSM-5 provided a low total yield of acrolein and acrylic acid,

17   suggesting that molybdenum and/or vanadium oxides on Mo-V/ZSM-5 catalyzed

17

1 complete oxidation. Therefore, heteropoly acids loaded on ZSM-5 zeolite can catalyze

2 the efficient selective oxidation of acrolein into acrylic acid.

3 Fig. S4 shows time course of the catalytic activity of PV_2Mo_{10}/ZSM-5 for a long

4 time. The conversion did not change. Acrylic acid was observed at a selectivity of 30 %

5 after 6 h, but the selectivity decreased to 10 % at 72 h. The selectivity of acrolein increased.

6 The behaviors of acetic acid and acetaldehyde on time course were similar to those of

7 acrylic acid and acetaldehyde, respectively. Total selectivity of CO and CO_2, shown as

8 CO_x, slightly increased from 23 % at 1 h to 27 % at 72 h. The undetected product with

9 FID- and TCD-GC systems were described as others, and decreased from 33 % at 1 h to

10 2 % at 72 h. The behavior of others on time course was similar to that of acrylic acid. It

11 was speculated that others was carbon deposit on heteropoly acids, therefore the

12 deactivation of oxidation activity were related to the formation of carbon deposit on

13 PV_2Mo_{10}. Fig. S5 shows temperature dependence of glycerol oxidehydration over

14 PV_2Mo_{10}/ZSM-5 at 6h of time on stream. In the above, the reaction was carried out at

15 623 K. Selectivity of acrylic acid in the reaction at 603 K was lower than that of acrolein.

16 In contrast with the values at 623 K, selectivity of acrylic acid at 643 K decreased but that

17 of acrolein increased, therefore the oxidation activity decreased against ramping

18

1   temperature. It was speculated that formation rate of carbon deposit in the reaction at 643

2   K was faster than 623 K, therefore the oxidation activity declined.

3

4   3.3 *In-situ* IR analysis of adsorption and reaction by the catalysts

5   *In-situ* IR analysis was employed to observe acrolein adsorbed on the surface of the

6   catalysts and its desorption and/or conversion into products. The samples were pretreated

7   at 373 K for 1 h in vacuum. After introduction of acrolein into an IR cell at 303 K, the

8   cell was evacuated and gradually ramped from 303 to 673 K as IR spectra were recorded

9   at each temperature. **Fig. 8** shows difference IR spectra in which the spectrum before

10   acrolein adsorption at 303 K is subtracted from the corresponding spectrum at elevated

11   temperature to 323 K after acrolein adsorption at 303 K. In the spectrum for

12   PV_2Mo_{10}/SiO_2 (**Fig. 8** (a)), weak bands observed at 1710, 1660, 1625 and 1365 cm^{-1} were

13   assigned to ν (C=O) of a carbonyl-bonded compound linked with an O atom of a

14   heteropoly acid, ν (C=O) of a compound coordinated with a metal atom of a heteropoly

15   acid, C=C stretching, and CH_2 bending vibration, respectively [29]. In the IR spectra

16   measured at elevated temperatures up to 673 K (Fig. S6 (a)), the band at 1660 cm^{-1}

17   immediately decreased as the temperature increased, and the band at 1710 cm^{-1} gradually

18   disappeared. A broad band at 1480–1580 cm^{-1} was observed at 673 K and probably

1   assigned to the C=C stretching vibration of aromatic compounds, since the sample disk

2   changed from yellow to gray during IR analysis. The spectrum of ZSM-5 without

3   heteropoly acid (**Fig. 8** (b)) shows bands at 1675, 1605, 1460 and 1365 cm^{-1}, attributed

4   to ν (C=O) of a compound coordinated with Brønsted acid sites, C=C stretching, C‑H

5   rocking of the COH of aldehyde, and CH_2 bending vibration, respectively [30]. These

6   vibration modes were observed at 323-373 K (Fig. S6 (b)). The bands at 1730 and 1555

7   cm^{-1} were assigned to ν(C=O) of aldehyde in polymers formed through 1, 2-addition of

8   acrolein and to cyclic structures formed by the auto-condensation of aldehyde. As the

9   temperature increased, these structures gradually transformed into aromatics. Acrolein

10   molecules interacted with the Brønsted acid sites on ZSM-5 zeolite were activated, and

11   this interaction was likely stronger than that of acrolein with heteropoly acids.

12   Bands associated with acrolein absorption onto ZSM-5 were present in the spectra of

13   ZSM-5 zeolites modified with heteropoly acids and Mo-V mixed oxide. The vanadium

14   content of heteropoly acids affected the intensity ratio of several bands. PMo_{12}/ZSM-5,

15   which contained a smaller amount of Brønsted acid sites than ZSM-5 zeolite alone, had

16   a weaker band at 1675 cm^{-1}, assignable to ν(C=O) of a compound coordinated with the

17   Brønsted acid sites (**Fig. 8** (c)). The band at 1695 cm^{-1} was ascribable to ν (C=O) of a

18   coordinated species on molybdenum oxides derived from the decomposition of

20

1   heteropoly acids. An increase in the vanadium content increased the band intensity at

2   1675 cm^{-1}; this intensity was maximum for PV$_2$Mo$_{10}$ (**Fig. 8** (e)) due to adsorption of

3   acrolein on the acid sites of ZSM-5 and the stable heteropoly acids, as shown in the

4   Raman spectra. Fig. S6 (c)-(f) shows the IR spectra of ZSM-5 zeolite modified with

5   heteropoly acids at elevated temperatures up to 673 K, and Fig. S6 (h) shows the

6   difference IR spectra of PV$_2$Mo$_{10}$/ZSM-5 without adsorbed acrolein. The bands

7   assignable to acrolein adsorbed on PV$_2$Mo$_{10}$/ZSM-5 gradually weakened as the

8   temperature increased and a broad band at 1480–1580 cm^{-1} appeared, probably

9   attributable to the C=C stretching vibration of aromatic compounds. The spectra of other

10   heteropoly acids loaded on ZSM-5 zeolite also showed immediate decreases in the

11   intensities of acrolein bands and the appearance of the 1480–1580 cm^{-1} band arising from

12   aromatic compounds. In addition, *in-situ* IR analysis was used to characterize acrylic acid

13   adsorbed on the surface of ZSM-5 and PV$_2$Mo$_{10}$/ZSM-5 (Fig. S7). The bands attributed

14   to acrylic acid decreased immediately on spectra for the catalysts. Acrylic acid on the

15   catalyst surface may be desorbed at lower temperature compared to acrolein. Probably

16   due to this, the formation of acrylic acid was not observed on the catalysts during *in-situ*

17   IR analysis of acrolein adsorption (**Fig. 8**).

1   It is suggested that inhibition of polymerization and auto-condensation of acrolein

2   molecules was needed to increase selectivity of acrylic acid in the oxidehydration of

3   glycerol. The IR analysis thus indicated that these side reactions were inhibited on

4   PV_2Mo_{10}/ZSM-5 compared to the other catalysts, and therefore PV_2Mo_{10}/ZSM-5 showed

5   high catalytic activity and high selectivity of acrylic acid.

6

4. Conclusion

The oxidehydration of glycerol into acrylic acid was studied on a bifunctional catalyst formed from Keggin-type molybdovanadophosphoric acid and ZSM-5 zeolite. The heteropoly acid was dispersed on the stable ZSM-5 zeolite. Based on Raman analysis, PV_2Mo_{10} and PV_3Mo_9 on the zeolite retained the original structure of the Keggin-type heteropoly acids, but the structures of PMo_{12} and $PVMo_{11}$ partially decomposed. The amount of Brønsted acid sites on PV_2Mo_{10}/ZSM-5 and PV_3Mo_9/ZSM-5 was higher than those on PMo_{12}/ZSM-5 and $PVMo_{11}$/ZSM-5. The total yields of acrylic acid and acrolein in the catalytic oxidehydration of glycerol on PV_2Mo_{10}/ZSM-5 were about 60%, and the catalytic activity of PV_2Mo_{10}/ZSM-5 was higher than that of either a mixed bed or separate beds of ZSM-5 and PV_2Mo_{10}/SiO_2, or of Mo-V/ZSM-5. *In-situ* IR analysis suggested that acrolein molecules adsorbed on PV_2Mo_{10}/ZSM-5 were converted into acrylic acid due to inhibition of side-reactions such as polymerization and auto-condensation, which induced coke formation, compared to other heteropoly acids loaded on ZSM-5 zeolite investigated in this study.

Acknowledgements

23

1 Reference

[1] L. C. Meher, D. V. Sagar, S. N. Naik, Renew. Sustain. Energy Rev. 10 (2006) 248–268.

[2] C. A. G. Quispe, C. J. R. Coronado, J. A. Carvalho Jr., Renew. Sustain. Energy Rev. 27 (2013) 475–493.

[3] B. Katryniok, S. Paul, V. Bellière-Baca, P. Rey, F. Dumeignil, Green Chem., 12 (2010) 2079-2098.

[4] C.S. Callam, S. J. Singer, T.L. Lowary, C.M. Hadad, J. Am. Chem. Soc. 123 (2001) 11743-11754.

[5] A. Witsuthammakul, T. Sooknoi, Appl. Catal., A 413−414 (2012) 109−116.

[6] X. Feng, B. Sun, Y. Yao, Q. Su, W. Ji, C.-T. Au, J. Catal. 314 (2014) 132−141.

[7] P. Kampe, L. Giebeler, D. Samuelis, J. Kunert, A. Drochner, F. Haaß, A.H. Adams, J. Ott, S. Endres, G. Schimanke, T. Buhrmester, M. Martin, H. Fuess, H. Vogel, Phys. Chem. Chem. Phys. 9 (2007) 3577−3589.

[8] M. Dolores Soriano, P. Concepcion, J.M. López Nieto, F. Cavani, S. Guidetti, C. Trevisanut, Green Chem., 13 (2011) 2954−2962.

[9] F. Wang, J. Xu, J.-L. Dubois, W. Ueda, ChemSusChem 3 (2010) 1383−1389.

[10] L. Shen, H. Yin, A. Wang, X. Lu, C. Zhang, Chem. Eng. J. 244 (2014) 168−177.

[11] A. Chieregato, M. Dolores Soriano, F. Basile, G. Liosi, S. Zamora, P. Concepción, F. Cavani, J.M. López Nieto, Appl. Catal. B 150-151 (2014) 37−46.

[12] Y.S. Yun, K.R. Lee, H. Park, T.Y. Kim, D. Yun, J.W. Han, J. Yi, ACS Catal. 5 (2015) 82-94.

[13] A.S. Paula, L.G. Possato, D.R. Ratero, J. Contro, K. Keinan-Adamsky, R.R. Soares, G. Goobes, L. Martins, J.G. Nery, Microporous Mesoporous Mater. 232 (2016) 151-160.

[14] J. Tichý, Appl. Catal. A 157 (1997) 363-385.

[15] S. Suganuma, T. Hisazumi, K. Taruya, E. Tsuji, N. Katada, ChemisrySelect, 2 (2017) 5524-5531.

[16] L.G. Possato, W.H. Cassinelli, T. Garetto, S.H. Pulcinelli, C.V. Santilli, L. Martins, Appl. Catal., A 492 (2015) 243–251.

[17] X. Li, Y. Zhang, ACS Catal. 6 (2016) 2785-2791.

[18] S. Suganuma, Y. Murakami, J. Ohyama, T. Torikai, K. Okumura, N. Katada, Catal. Lett. 145 (2015) 1904-1912.

[19] P. K. Dutta, M. Puri, J. Phys. Chem., 91 (1987) 4329-4333.

[20] F. Fan, K. Sun, Z. Feng, H. Xia, B. Han, Y. Lian, P. Ying, C. Li, Chem. Eur. J., 15 (2009) 3268 – 3276

[21] G. Mestl, T. Ilkenhans, D. Spielbauer, M. Dieterle, O. Timpe, J. Kröhnert, F. Jentoft, H. Knözinger, R. Schlögl, Appl. Catal. A Gen., 210 (2001) 13-34.

[22] H. Liu, E. Iglesia, J. Catal. 223 (2004) 161-169.

[23] L. Zhou, L. Wang, S. Zhang, R. Yan, Y. Diao, J. Catal. 329 (2015) 431-440.

[24] G. Mestl, J. Raman Spectrosc. 33 (2002) 333-347.

[25] B. Solsona, A. Dejoz, T. Garcia, P. Concepción, J.M. López Nieto, M.I. Vázquezb, M.T. Navarro, Catal. Today 117 (2006) 228-233.

[26] M. Niwa, N. Katada, K. Okumura, Characterization and Design of Zeolite Catalysts: Solid Acidity, Shape Selectivity and Loading Properties, Springer, Berlin, 2010, p. 29-59.

25

[27] W. Suprun, M. Lutecki, T. Haber, H. Papp, J. Mol. Catal. A 309 (2009) 71-78.

[28] Y. S. Yun, K. R. Lee, H. Park, T. Y. Kim, D. Yun, J. W. Han, J. Yi, ACS Catal. 5 (2015) 82-94.

[29] G. Ya. Popova, T. V. Andrushkevich, I. I. Zakharov, Yu. A. Chesalov, Kinet. Catal. 46 (2005) 217-226

[30] E. Yoda, A. Ootawa, Appl. Catal. A: Gen. 360 (2009) 66-70.

1

1 **Table 1.**   Amount of Brønsted acid sites on the catalysts

Sample	Amount of Brønsted acid site / mol kg^{-1}
ZSM-5 [a]	0.30
PMo$_{12}$/ZSM-5 [a,b]	0.19
PVMo$_{11}$/ZSM-5 [a,b]	0.23
PV$_2$Mo$_{10}$/ZSM-5 [a,b]	0.32
PV$_3$Mo$_9$/ZSM-5 [a,b]	0.32
Mo-V/ZSM-5 [a,b]	0.31
PV$_2$Mo$_{10}$/SiO$_2$	0.00

[a] H-type, Si/Al = 45. [b] ([Mo] +[V])/[Al] = 3.0.

2

Figure Captions

Fig. 1 XRD patterns of (a) ZSM-5, (b) PMo_{12}/ZSM-5, (c) $PVMo_{11}$/ZSM-5, (d) PV_2Mo_{10}/ZSM-5, (e) PV_3Mo_9/ZSM-5, (f) Mo-V/ZSM-5, (g) SiO_2 and (h) PV_2Mo_{10}/SiO_2.

Fig. 2 N_2 adsorption-desorption isotherms at 77 K of (a) ZSM-5, (b) PMo_{12}/ZSM-5, (c) $PVMo_{11}$/ZSM-5, (d) PV_2Mo_{10}/ZSM-5, (e) PV_3Mo_9/ZSM-5 and (f) Mo-V/ZSM-5.

Fig. 3 SEM images and the corresponding EDX mapping images of (a) PV_2Mo_{10}/ZSM-5 and (b) ZSM-5.

Fig. 4 Raman spectra of (a) ZSM-5, (b) PMo_{12}/ZSM-5, (c) $PVMo_{11}$/ZSM-5, (d) PV_2Mo_{10}/ZSM-5, (e) PV_3Mo_9/ZSM-5, (f) PV_2Mo_{10}/SiO_2 and (g) Mo-V/ZSM-5.

Fig. 5 Time course of catalytic activities of PV_xMo_{12-x}/ZSM-5 (17-18 wt%) in the oxidehydration of glycerol. (a) Conversion and yields of (b) acrolein, (c) acrylic acid, (d) acetaldehyde and (e) acetic acid.

Fig. 6 Influence of loading amount of PV_2Mo_{10}/ZSM-5 on the conversion and yield of products in the oxidehydration of glycerol at 6 h of time on stream.

Fig. 7 Comparative yields of catalytic reaction systems for the oxidehydration of glycerol. (a) Conversion and yields of (b) acrolein, (c) acrylic acid, (d) acetaldehyde and (e) acetic acid.
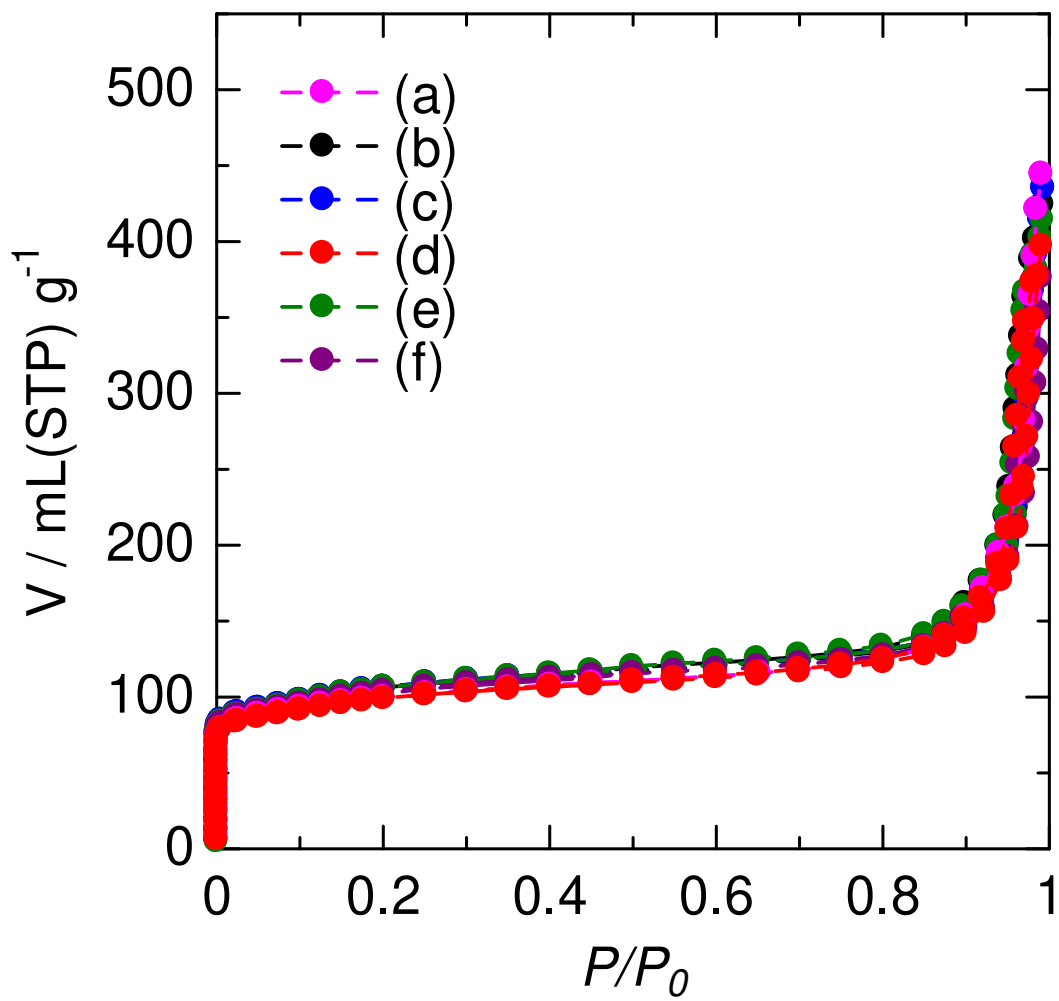
1 [The systems: PV_2Mo_{10}/ZSM-5, Mo-V/ZSM-5, PV_2Mo_{10}/SiO$_2$ (13.6 wt%), mixed bed

2 (ZSM-5 zeolite + PV_2Mo_{10}/SiO$_2$ (13.6 wt%)) and separate bed (1st bed: ZSM-5 zeolite,

3 2nd bed: PV_2Mo_{10}/SiO$_2$ (13.6 wt%))]

4 **Fig. 8**   Difference IR spectra: (spectrum after acrolein adsorption and raising the

5 temperature to 323 K) – (spectrum before acrolein adsorption). (a) PV_2Mo_{10}/SiO$_2$, (b)

6 ZSM-5, (c) PMo_{12}/ZSM-5, (d) $PVMo_{11}$/ZSM-5, (e) PV_2Mo_{10}/ZSM-5, (f) PV_3Mo_9/ZSM-

7 5 and (g) Mo-V/ZSM-5.

Fig. 1

Fig. 2

1

2

3

Fig. 3

Fig. 4

Fig. 5

Fig. 6

Fig. 7

Fig. 8

1

2